Surface Modification with Alginate-Derived Polymers for Stable, Protein-Repellent, Long-Circulating Gold Nanoparticles

Anu Kodiyan,[†,‡] Eduardo A. Silva,[†,§,¶] Jaeyun Kim,[†,⊥,∥] Michael Aizenberg,[†] and David J. Mooney[†,⊥,*]

[†]Wyss Institute for Biologically Inspired Engineering, Harvard University, Cambridge, Massachusetts 02138, United States, [‡]École Polytechnique Fédérale de Lausanne, 1015 Lausanne, Switzerland, [§]Department of Biomedical Engineering, University of California, Davis, California 95616, United States, [⊥]School of Engineering and Applied Sciences, Harvard University, Cambridge, Massachusetts 02138, United States, and [∥]School of Chemical Engineering, Sungkyunkwan University, Suwon 440-746, Korea. [¶]Present address: Department of Biomedical Engineering, University of California, Davis, 451 East Health Sciences Drive, Davis, CA 95616.

ABSTRACT

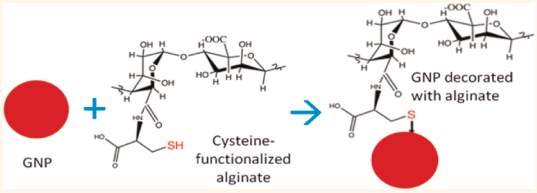

Poly(ethylene) glycol is commonly used to stabilize gold nanoparticles (GNPs). In this study, we evaluated the ability of cysteine-functionalized alginate-derived polymers to both provide colloidal stability to GNPs and avoid recognition and sequestration by the body's defense system. These polymers contain multiple reactive chemical groups (hydroxyl and carboxyl groups) that could allow for ready functionalization with, for example, cell-targeting ligands and therapeutic drugs. We report here that alginate-coupled GNPs demonstrate enhanced stability in comparison with bare citrate-coated GNPs and a similar lack of interaction with proteins *in vitro* and long *in vivo* circulation as PEG-coated GNPs.

KEYWORDS: G-block · PEG · protein repellence · thiol polymers · cellular uptake · pharmacokinetics

There is increasing interest in the use of gold nanoparticles (GNPs) for various applications in biomedical materials science, electronics, and optics as they possess unique key features.[1] In particular, they have been shown to have excellent biocompatibility,[2] making them suitable for biomedical applications. Gold has been approved by the United States Food and Drug Administration for use in humans for rheumatoid arthritis and has been safely used for over 60 years.[3−5] GNPs can easily be conjugated to other molecules due to gold's high affinity for thiols, amines, and phosphines.[6] In addition, GNPs present tremendous potential in biomedical imaging. For instance, they have been shown to induce specific contrast enhancement in X-ray computed tomography.[7] These properties make them valuable tools for applications such as therapeutic drug delivery, cancer diagnostics, and therapy.[8] Currently, spherical GNPs are most commonly made using the method proposed by Frens[9] in 1973 by the reduction of chloroauric acid to neutral gold by sodium citrate. The challenge with the use of these GNPs for *in vivo* applications is that unmodified GNPs undergo aggregation induced by the high ionic strength and serum proteins in body fluids, resulting in rapid elimination from the systemic circulation by cells of the reticuloendothelial system (RES).[10] The most commonly used stabilizing agents for GNPs are the water-soluble polyethylene glycol (PEG) molecules, as they provide excellent stability and significantly increase *in vivo* circulation time of the coated particles in comparison with plain GNPs.[11] PEGylation of GNPs is typically performed by using thiol (SH)-terminated PEGs, exploiting the very high specific bonding affinity of gold to thiol groups.[12] The rationale underlying this approach is that coating the GNP surface with hydrophilic polymers can significantly reduce nonspecific interactions with biomolecules such as plasma proteins. Indeed, materials designed for use in the human body should ideally be nonimmunogenic and have protein-repellent surfaces to avoid inflammation or thrombus formation upon contact of the material with blood.[13] Although PEG molecules provide excellent stability to GNPs, their non-ionic

* Address correspondence to mooneyd@seas.harvard.edu.

Received for review December 25, 2011 and accepted May 31, 2012.

Published online May 31, 2012
10.1021/nn205073n

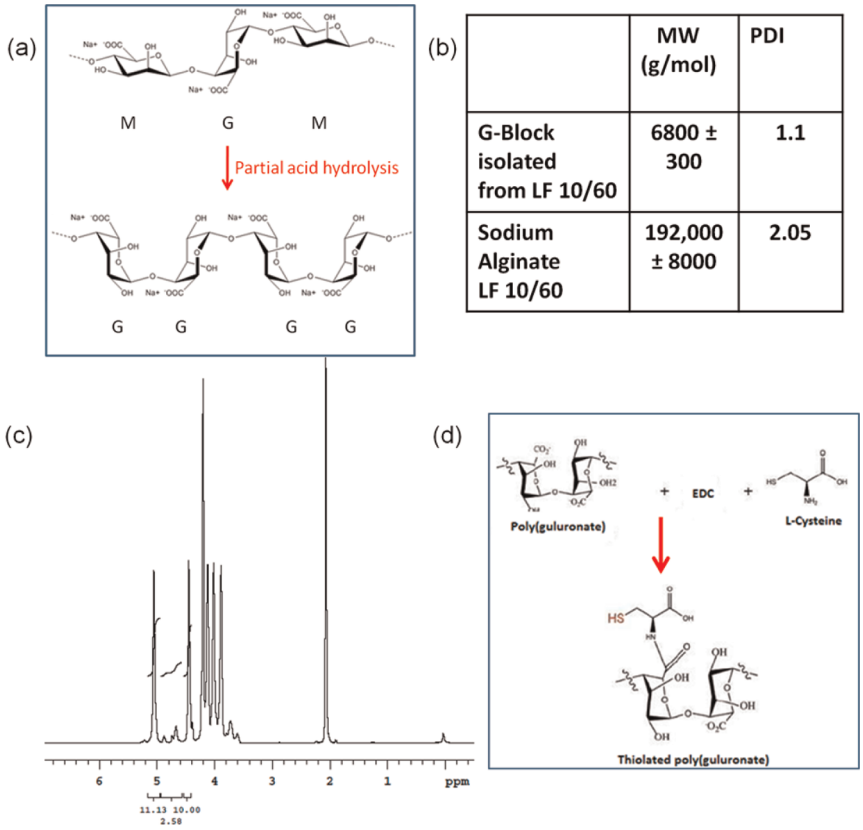

	MW (g/mol)	PDI
G-Block isolated from LF 10/60	6800 ± 300	1.1
Sodium Alginate LF 10/60	192,000 ± 8000	2.05

Figure 1. (a) G-block polymers were synthesized from sodium alginate (LF10/60) by partial acid hydrolysis. (b) GPC results indicating the molecular weight (MW) and the polydispersity index (PDI) of the polymers tested. (c) Proton NMR spectra of G-block polymer indicating that the G-block polymers isolated from alginate LF10/60 had approximately 88% guluronic acid content. (d) Cysteines were incorporated to G-block polymers *via* EDC chemistry (G-block/cysteine molar ratio of 1:1.75).

and inert nature[14] limit their potential for chemical functionalization. PEG is activated for coupling by preparing a derivative having a functional group at one or both termini,[15] hence PEGs are attached to other molecules only *via* their terminal ends.

In this study, we explored whether polymers derived from alginate can serve as alternative stabilizing agents for GNPs. These polymers offer the possibility of chemically (*via* covalent interactions)[16,17] or physically (*via* ionic interactions)[18,19] associating many different molecules, including growth factors[20] and cell-adhesive ligands to alginate.[21] Indeed, alginate polymers can be extensively functionalized thanks to the presence of multiple reactive chemical groups (carboxyl and hydroxyl groups). There are several attractive reasons to engineer alginate polymers for therapeutic applications: they are well-characterized, amenable to sterilization and storage, biocompatible with human tissues,[22] and possess unique gel-forming properties and pH-dependent charges. Alginates are naturally derived polysaccharides, composed of (1−4)-linked β-D-mannuronic acid (M-units) and α-L-guluronic acid (G-units) sugar residues.[23] The alginate molecule is a block copolymer with regions of sequential M-units, called M-blocks, regions of sequential G-units, called G-blocks, and regions of atactically organized M- and G-units. Divalent cations, such as Ca^{2+}, bind between the G-blocks of adjacent alginate chains, allowing gelation of aqueous alginate solutions.[24] A very attractive feature of alginate is that it is commonly considered to be a non-immunogenic polymer.[25−27] The GNPs were thus coated with alginate-derived polymers to both provide colloidal stability and avoid recognition and sequestration by the body's defense system. In this study, GNPs coated with cysteine-functionalized G-block polymers and low molecular weight alginate polymers were analyzed for their physical properties, *in vitro* characteristics, and *in vivo* blood circulation. Furthermore, GNPs coated with alginate-derived molecules were compared to PEGylated GNPs. Results obtained with G-block-coated GNPs are highlighted, and results obtained with low molecular weight alginate-coated and PEGylated GNPs are provided in the Supporting Information.

RESULTS AND DISCUSSION

Polymer Characterization. Poly(guluronate) (G-blocks) was isolated from sodium alginate LF10/60 (ProNova Biomedical, FMC, Norway) according to the procedure described by Bouhadir *et al.*[28] (Figure 1a). Gel permeation chromatography (GPC) analysis indicated that the isolation of G-blocks from alginate resulted in polymers

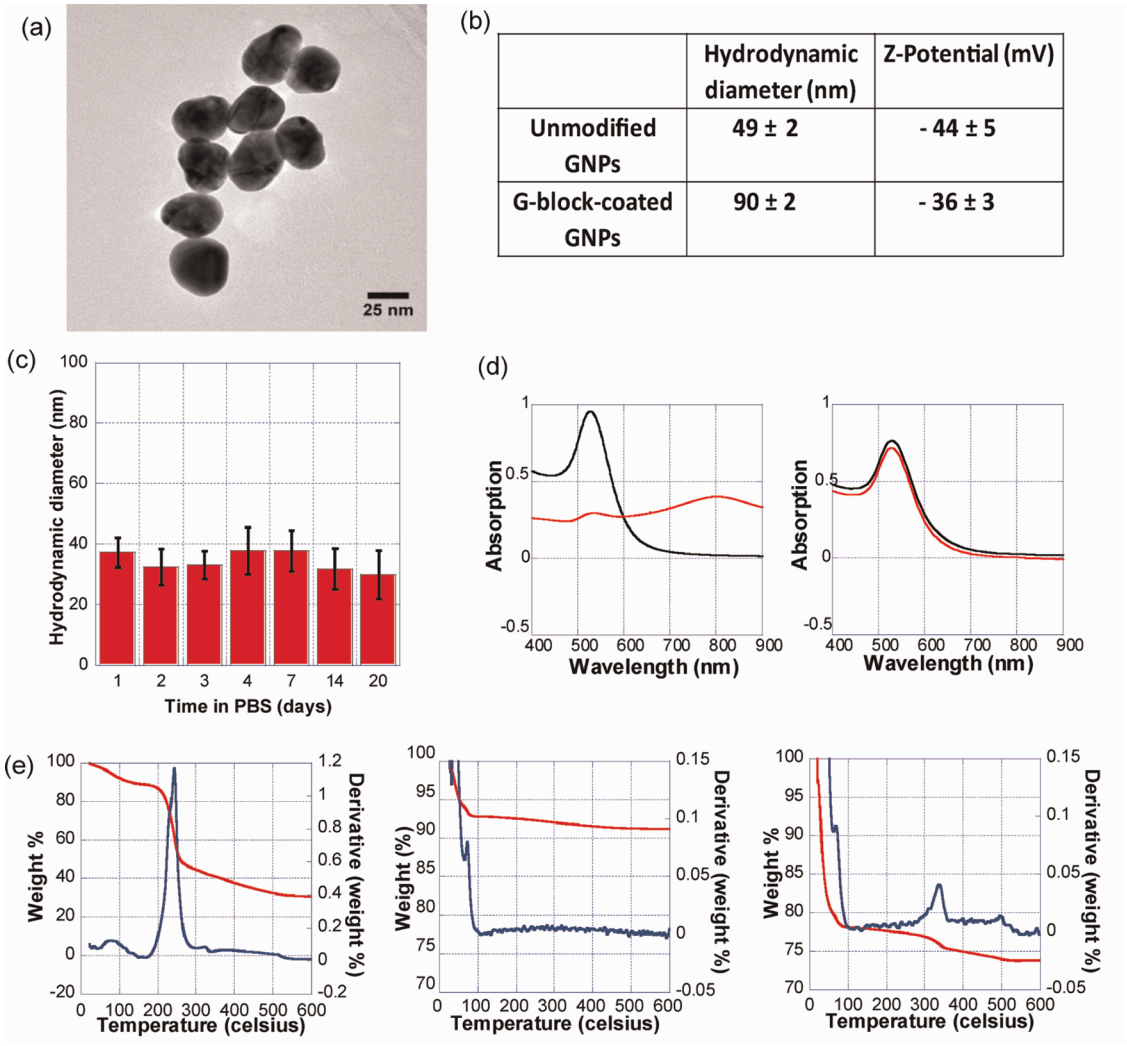

	Hydrodynamic diameter (nm)	Z-Potential (mV)
Unmodified GNPs	49 ± 2	- 44 ± 5
G-block-coated GNPs	90 ± 2	- 36 ± 3

Figure 2. (a) TEM image of GNPs indicating that the GNPs had diameters of approximately 25 nm. (b) Hydrodynamic diameter and zeta-potential of GNPs of unmodified and G-block-coated GNPs. (c) Hydrodynamic diameters of G-block-coated GNPs resuspended in PBS, indicating that the GNPs had a stable size over 20 days (values represent mean (n = 5) and standard deviation). (d) Absorption spectra of unmodified GNPs (left) and G-block-coated GNPs (right) in PBS (red curve) and in water (black curve). (e) TGA profiles of G-block polymer (left), unmodified GNPs (center), and G-block-coated GNPs (right). Weight %: red curve. Derivative (wt %): blue curve.

with significantly reduced molecular weight and viscosity (Figure 1b) in comparison with the alginate molecules from which they were isolated. The MW of the monomers constituting alginate, guluronic acid, and mannuronic acid in its deprotonated form ($C_6H_7O_6$) is 176.1 g/mol. Hence, there are approximately (6800/176.1) 38 units of guluronic acids in the G-block polymer isolated from LF10/60. It has been reported that a minimum chain length of approximately 18 guluronic acid units is needed for cooperative G-block dimerization at certain *in vitro* binding conditions[29] and that the gelation and the strength of dimerization resulting from G-block dimerization increase with block length.[30] Hence, the length of the G-block molecules isolated from alginate LF10/60 is long enough to induce gelation of the polymers for potential future applications, such as trapping G-block-coated GNPs in target areas of the body by *in situ* gelation. Indeed, high Ca^{2+} concentrations are naturally present in the interstitial volume of the body. The guluronic acid percentage of the G-block polymers was calculated from proton nuclear magnetic resonance (^{1}H NMR) spectra using a literature method[31−33] (Figure 1c) and confirmed that G-block polymers contain ~88% guluronic acids on average. G-blocks isolated in this manner also had very low endotoxin content (<0.02 EU/mL), hence these polymers could safely be used for *in vivo* studies.

Cysteines were incorporated into the alginate-derived polymers (Figure 1d) to provide them with thiol functional groups, which can react with gold nanoparticles, by using previously described synthesis of alginate−cysteine conjugates.[34] Inductively coupled plasma mass spectrometry (ICP-MS) indicated that G-block polymers had 0.0194% sulfur content (obtained by Galbraith Laboratories, Inc.). Low degrees of substitution were selected for the addition of thiols

on the polymers to prevent thiols of the same polymer from binding to different GNPs and agglomerating GNPs. In fact, at much higher degrees of thiol substitution, agglomerated clusters of GNPs coated with G-blocks were visible to the naked eye. Although oxidation could naturally occur and thus cause the polymers to contain disulfide bonds, it has been reported that the formation of self-assembled monolayers from either thiols (RSH) or analogous disulfide adsorbates (RSSR) on gold both yield monolayers of similar structure.[35]

GNP Characterization. To develop a nanoparticle-based drug delivery system, size and surface charge are crucial parameters that will determine the biodistribution, pharmacokinetics, toxicity, and tumor penetration potential. Ideally, the nanoparticle size should be above 10 nm to avoid renal clearance[36] and below 100 nm with a neutral or negative charge to avoid clearance by phagocytic uptake and hepatic filtration.[37] Particles smaller than 100 nm easily penetrate tumor tissues as the size of their fenestra is approximately 100 nm.[38] Transmission electron microscopy (TEM) imaging revealed that GNPs had an average diameter of 25 nm (Figure 2a). Dynamic light scattering indicated that coating the GNPs with G-block polymers increased the hydrodynamic size of the GNPs in comparison with unmodified GNPs, while zeta-potential measurements indicated that both unmodified GNPs and GNPs coated with G-block polymers were negatively charged (Figure 2b). The difference in the TEM and DLS measurements is attributed to the polymer on the GNPs. Hydrodynamic sizes of the polymer-coated GNPs were greater than those determined by TEM due to the formation of protective layers of polymer bound covalently to the surface of the particles. These zeta-potential results are consistent with literature reports that plain spherical GNPs are negatively charged.[39] Guluronic and mannuronic acids are negatively charged at neutral pH due to the presence of carboxyl groups,[40] hence G-block-coated GNPs remain negatively charged. Interestingly, the zeta-potential measurements indicated that, prior to the functionalization, GNPs are more negatively charged than GNPs coated with the negatively charged G-block polymers. This is likely because functionalization with the G-block polymers is in fact a displacement by them of many negatively charged citrate ions, which results in reorganization of the surface charge of the particles and the corresponding change in zeta-potential. For potential applications such as specific cell targeting, the negative charge of the particles could help to reduce nonspecific uptake since interactions with negatively charged membranes on cells are less favorable. It has been demonstrated that neutral and negatively charged gold nanoparticles adsorbed much less on the negatively charged cell membrane surface, in comparison with positively charged particles.[41] Interestingly, negatively charged carboxyl groups on the surface of the nanoparticles have been reported to be less toxic than positively charged amine groups on the nanoparticle surface.[42] This observation is insightful for the use of alginate-derived polymers as GNP coating agents since they contain a carboxyl group on each sugar residue in the polymer.

It is known that aggregation of GNPs occurs when the electrostatic repulsive forces produced by the negative surface of the GNPs are outbalanced by the van der Waals attractive forces between the particles.[43] To verify if nanoparticle aggregation occurs in conditions which would challenge the electrostatic repulsive forces between the particles, GNPs were centrifuged and suspended in phosphate buffered saline (PBS). Hydrodynamic diameter measurements of the modified GNPs in PBS indicated they have a stable size for 20 days after being resuspended in PBS (Figure 2c), unlike unmodified GNPs for which hydrodynamic measurements revealed a size of 625 nm, clearly indicating severe aggregation. This observation supports the assumption that coating the particles with cysteine-functionalized alginate-derived polymers provides extra stability to the GNPs in comparison with the unmodified GNPs. Another way of verifying the stability of the particles is by UV−vis absorption measurements. The plasmon resonance absorption band is an excellent probe for monitoring aggregation of GNPs because of its high sensitivity toward the dielectric environment of the metal nanoparticles. It is known that, upon aggregation of the particles, an intense long-wavelength band (>600 nm) will develop.[44] Monodisperse GNPs of 25 nm diameter have a peak of absorption at 525 nm and have a red color when they are kept in neutral solvents such as water. Typically, unmodified GNPs spontaneously turn gray when they are centrifuged and resuspended in PBS, indicating agglomeration of the particles. Measurements of the absorption of the suspensions of GNPs were taken and compared with those of unmodified GNPs (Figure 2d) both in water and in PBS. When G-block-coated GNPs were resuspended in PBS, they retained a peak of absorption at 525 nm, confirming that GNPs coated with G-block polymers are more stable than unmodified GNPs. To verify if the enhanced stability of GNPs in the presence of G-block polymers is indeed due to the covalent Au−S bonds, G-block polymers with extremely low degrees of thiol substitution (DS = 0.2, DS = 0) were tested as well and did not provide any stability to the GNPs, as they spontaneously turned dark blue when resuspended in PBS, confirming that there is a critical minimum DS needed to ensure the covalent binding of the G-blocks to the GNPs that results in their stabilization.

In order to estimate the number of G-block polymers per GNP, thermogravimetric analysis (TGA) was performed for the cysteine-functionalized G-block polymer, unmodified GNPs, and G-block-coated GNPs

(Figure 2e). Weight loss at temperatures below 100 °C corresponds to evaporation of water in the samples. TGA of the cysteine-functionalized G-block polymer indicates that there is some residual weight that cannot be eliminated even by increasing the temperature up to 600 °C. This residual weight corresponds to the presence of salts, which originate from the synthesis of the polymer, as the polymers were dissolved in MES/NaCl buffer during the cysteine attachment to the polymers. TGA qualitatively reveals the covalent attachment of polymers on the surface of the GNPs. In the case of unmodified GNPs, there is no significant weight loss in comparison with the polymer-coated GNPs. The small weight loss observed with the unmodified GNPs as the temperature was raised from 100 to 600 °C (1.6 ± 0.04%) corresponds to the citrate molecules which were added as stabilizing surfactant as per the synthesis of the GNPs. The derivative of the weight % *versus* temperature indicates at what temperature the highest weight loss occurs. By comparing the TGA measurements of the polymer alone with those of the polymer-coated GNPs, one can observe that the temperatures for burning off the polymers which are attached to the GNPs is significantly higher than the temperature for burning off the polymer alone. Indeed, for G-block polymers that are not attached to gold nanoparticles, the major weight loss occurs around 250 °C. Upon attachment to the gold nanoparticles *via* thiol−gold covalent bonds, the temperature at which maximal weight loss occurs is shifted to 330 °C. This temperature shift indicates the strength of the chemisorption of the polymers onto the gold surface, and that more energy is required to break the covalent bonds and fully burn the polymer. In average, the weight loss between 100 and 600 °C for G-block-coated GNPs was 3.5 ± 0.7%. When it is assumed that all GNPs have a mean diameter of 25 nm and are of spherical shape, the weight of a single GNP is approximately 0.16 fg. Since the polymer was added in excess in comparison with the GNPs and was allowed to react for a long time, one can assume that the polymer will displace some of the weakly bound citrate molecules from the GNPs, upon binding to the GNPs. In the scenario where all of the citrate molecules are displaced, the weight of G-block polymers per GNP represents 3.5% of the GNP weight and hence is corresponding to approximately 495 G-block molecules bound to one GNP. In the scenario where none of the citrate molecules are displaced away, the weight of G-block polymers per GNP represents 1.9% of the GNP weight and hence is corresponding to approximately 270 G-block molecules bound to one GNP. Hence, the number of G-block polymers per GNP is probably at an intermediate number between 270 and 495. If each polymer is bound to the gold nanoparticle *via* its terminal end (tightly bound monolayer in brush structure), the theoretical number of polymers which would be able to bind to one GNP, equivalent to the total surface area of the gold nanoparticle divided by the parking area of the thiol headgroup,[45] is 445 molecules. Another possible configuration is that the polymers lay flat on the particle. If one assumes that the G-blocks are arranged as a flat layer, the number of G-block polymers that would be able to bind to the GNP would be equivalent to the surface area of the GNP divided by the polar surface area of the G-block molecule. According to Chemspider database, the polar surface of guluronic acid and mannuronic acid is 80.29 Å^2. Since the G-block polymers have approximately 38 guluronic acids, the total surface area of the G-block molecule is 3051 Å^2. In the flat layer assumption, the number of G-block molecules that should be able to bind to a single GNP is approximately 64. TGA measurements indicate that the G-block molecules are arranged in an intermediate conformation between brush and flat configurations. Although these calculations are based on several assumptions, which are nevertheless reasonable, the TGA measurements provide a good insight into the general configuration in which the G-block molecules are arranged on the particles. In comparison, TGA measurements of PEGylated GNPs clearly indicated that the PEG molecules were arranged in a brush structure, which is consistent with literature reports (see Supporting Information).

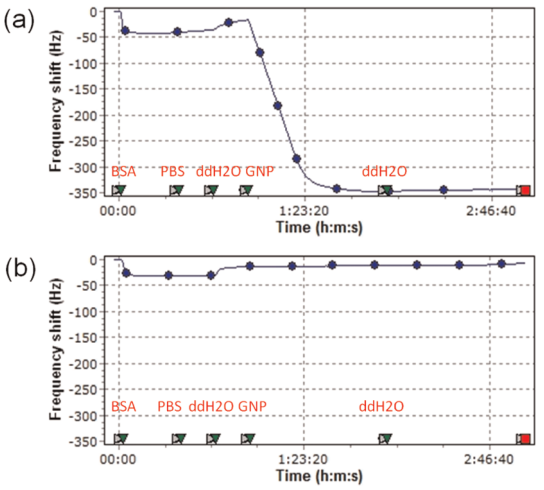

Figure 3. (a) QCM profile of unmodified GNPs: the significant drop in frequency shift upon the addition of GNPs indicates the strong adsorption of unmodified GNPs to serum proteins. (b) QCM profile of G-block-coated GNPs, indicating that G-block-coated GNPs do not adsorb to serum proteins.

***In Vitro* Characterization.** Quartz crystal microbalance (QCM) results indicated that unmodified GNPs strongly adsorb to bovine serum albumin (BSA) (Figure 3a), as there is a significant drop in the frequency shift once the sensor is exposed to the GNPs. Upon surface modification of the GNPs with G-blocks, the modified GNPs do not get adsorbed onto BSA (Figure 3b). Similarly, MVG-coated and PEGylated GNPs did not

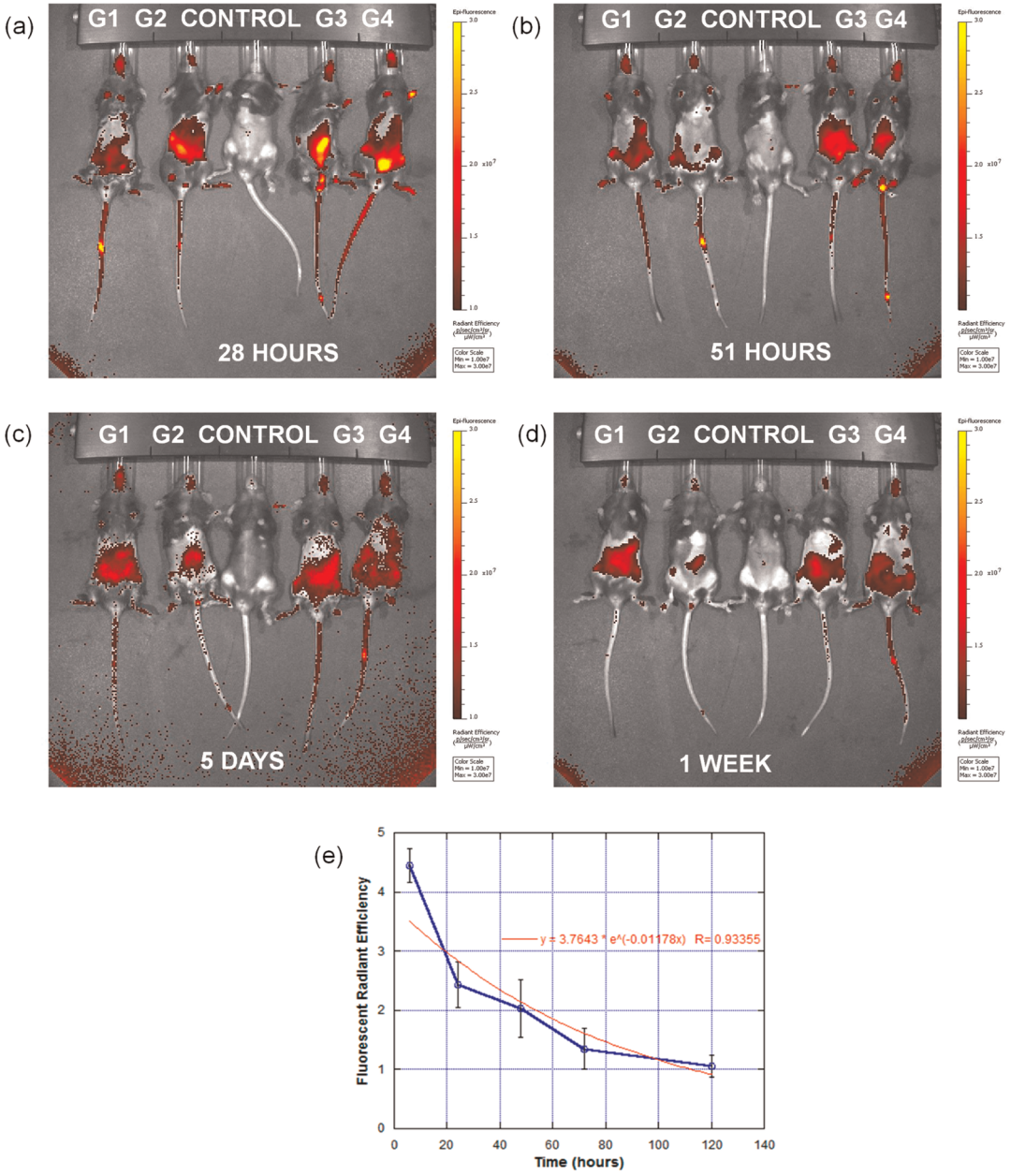

Figure 4. (a–d) *In vivo* fluorescence images of the mice taken at 28 h, 51 h, 5 days, and 1 week after retro-orbital injection of G-block-coated GNPs. (e) Pharmacokinetic profile of G-block GNPs, with exponential curve fit indicating that these GNPs had a half-life of 59 h in the peripheral blood of mice (values represent mean (n = 4), and standard deviation).

get adsorbed onto BSA (Supporting Information). This is consistent with what has been previously reported, as BSA binds spontaneously to the surface of citrate-coated GNPs primarily due to electrostatic interactions.[46] In general, the nonspecific binding of BSA to various gold surfaces coated with self-assembled monolayers is favored in the following order: hydrophobic > $-COO^-$ > $-NH_3^+$ > $-OH$ > ethylene glycol.[47−49] *In vivo*, nonspecific adsorption of proteins on the nanoparticle surface may cause (1) particle agglomeration and clearance from the RES, preventing the particles from delivering drugs to the target site, and (2) the nonspecific binding of the particles to cell membranes and the extracellular matrix, leading to inefficient tagging.[50]

It is generally known that coating surfaces with PEG molecules results in the reduction in adsorption of biomolecules on the surface-modified substrates. It is thought that the PEG layer might provide an interfacial barrier to prevent proteins from interacting with the underlying substrate, and this protein-rejecting property is thought to depend on several parameters, including PEG molecular weight, polymer chain architecture, and most importantly the interfacial PEG chain density.[51] Similarly, the alginate-derived polymers likely provide an interfacial barrier between the GNPs and the proteins, preventing their interaction. It is believed that serum proteins acting as opsonins contribute significantly to the interaction of macrophages

with particles.[52] The low affinity of the GNPs coated with alginate-derived polymers for the serum protein albumin is promising, as one of the primary ways GNPs are cleared from the body is by uptake of phagocytic cells mediated by protein interactions *via* complement receptors, mannose receptors, and Fc-γ receptors.[53] It is generally thought that when nanoparticles are introduced in the blood, serum albumin and fibrinogen dominate the particle surface for short periods of time, whereas lower-abundance proteins with higher affinities and slower kinetics might ultimately displace them.[54] In this context, for consideration of nonspecific protein adsorption on the surface of alginate-coated gold nanoparticles, we tested the affinity of the GNPs to serum albumin. Although there are more sensitive methods to measure the adsorption of proteins to nanoparticles, such as size-exclusion chromatography (SEC), isothermal titration calorimetry (ITC), and surface plasmon resonance (SPR),[54,55] QCM provides an alternative tool to qualitatively verify if the surface modification of the particles reduces the amount of protein that adsorbs to the GNPs,[56−58] which was the goal of this study. Furthermore, although several other proteins are known to bind to nanoparticles, the goal of this assay was to verify if the surface modification contributes to the reduction of protein adsorption in general in a similar way as PEG.

***In Vivo* Study.** Mice were injected with GNPs coated with cysteine-functionalized G-block polymers, which had been fluorescently labeled with NIR dye (Hylite 750, AnaSpec, Inc.). A control mouse is placed in the center of all the pictures, surrounded by mice that received G-block-conjugated GNPs (Figure 4a−d). The G-block-coated GNPs circulated in the peripheral blood for up to a week, but by 11 days the fluorescence radiant efficiency of the mice injected with the particles was nearly equivalent to that of the control mouse, suggesting that the GNPs were mostly cleared by that time (Supporting Information). The measured half-life of G-block GNPs was approximately 59 h. As a comparison, 20 nm GNPs coated with PEG (MW = 5000) have been reported to have a blood circulation half-life of approximately 32 h in BALB/cJ mice.[36] Unmodified spherical GNPs have been reported to be rapidly cleared, with only 0.004% of 15 nm GNPs, 0.002% of 50 nm GNPs, 0.0002% of 200 nm GNPs, and no detectable 100 nm GNPs remaining in the circulation at 24 h.[59] Hence, we can conclude that G-block molecules coated on the surface of the GNPs help to increase the circulation time of the GNPs in comparison with unmodified GNPs and this is most likely a result of (1) providing better stability to the nanoparticles and (2) reducing protein adsorption thus reducing clearance by macrophages in the RES. Other possibilities might explain the increased circulation time of the G-block-coated GNPs. For instance, *in vivo* gelation may have occurred between the different polymers in the presence of the Ca^{2+} ions that are naturally present in the interstitial volume, causing the particles to be cross-linked and to accumulate in various tissues of the body. However, this would have caused the particles to become greater in size and likely more rapidly recognized and eliminated. Further, pharmacokinetic measurements and the images of the mice injected with GNPs indicated that the GNPs were present in the peripheral blood. Future studies will be required to assess how these GNPs are altered upon introduction to the blood. G-block-coated GNPs may be quite useful for sophisticated drug delivery systems, due to the ready functionalization of the G-blocks and their gelling properties. One could target G-block-coated GNPs to specific tissues in the body where they could then be cross-linked thanks to high calcium concentrations in the interstitial volume and be trapped to deliver drugs in a sustained way. Furthermore, the pH-dependent charges of alginate could be exploited for controlling localization and transport of G-block GNPs.

CONCLUSION

In conclusion, we have shown that cysteine-functionalized alginate-derived polymers can be used to coat the surface of gold nanoparticles to increase the stability of the GNPs and reduce the adsorption of GNPs to proteins. The multiple functional groups of alginate-derived polymers allow ready functionalization with cysteines and fluorescent dyes. Furthermore, we observed that these modified GNPs circulated in the peripheral blood of mice for up to a week. Overall, this study describes a novel approach to coat the surface of gold nanoparticles providing a direct alternative that bypasses some of the well-known limitations of PEGylation as a means to stabilize nanoparticles and also holds great therapeutic potential for a variety of targeted drug delivery strategies thanks to the unique properties of alginate polymers.

METHODS

Gold Nanoparticle (GNP) Synthesis. GNPs were synthesized using the procedure reported by Frens.[9] A volume of 390 mL of double distilled water was used to dissolve 0.1 mmol of gold(III) chloride trihydrate and boiled under stirring conditions. Immediately after boiling, a volume of 10 mL of sodium citrate tribasic dihydrate solution (0.017 mM) dissolved in distilled water was quickly added. The final solution was readjusted to 400 mL with distilled water to compensate for evaporation, and the resulting concentration of the GNP solution was 0.04 mg/mL.

Gel Permeation Chromatography (GPC). GPC of the polymers was performed at 30 °C on a Viscotek GPCmax VE 2001 equipped with Viscotek TDA 305 triple detector array using 2 Viscotek A5000 columns (dimensions 300 × 7.9 mm) at a flow rate of 1 mL/min. The mobile phase and the solvent for the samples were composed of high purity water containing 1 g/L sodium

azide and 4.2 g/L sodium nitrate. The GPC was calibrated with a PEO standard purchased from American Polymer Standards Corp. (PEOX100K).

Preparation of the Samples for NMR. The samples were dissolved in D_2O (100% D) and repeatedly freeze-dried to ensure full isotope exchange and suppression of proton signals from H_2O and all other exchangeable protons. The solid polymer (10 mg) was then dissolved in 0.6 mL of D_2O to which acetonitrile (0.3%) was added as internal standard (σ = 2.06 for the acetonitrile methyl group). The ^{1}H NMR spectra (400 MHz, Varian Unity) measured at 80 °C and 100 scans (pulse angle = 63°, acquisition time = 3.744 s, and relaxation delay = 1 s) were obtained from Custom NMR Services, 77 Pine Ridge Drive, Ayer, MA 01432, USA.

Incorporation of Cysteines on Alginate-Derived Polymers. A 1% w/v polymer solution was prepared in MES (0.1 M)/NaCl (0.3 M) buffer in double distilled water. The polymer was chemically modified utilizing aqueous carbodiimide chemistry. A water-soluble carbodiimide, 1-ethyl-3-(3-dimethylaminopropyl)-carbodiimide (EDC) was added to the solution of polymer. This was followed by the addition of L-cysteine hydrochloride monohydrate. A molar ratio of 1:1.75 was used for G-block/cysteine, while a molar ratio of 1:5 was used for MVG/cysteine. After addition of L-cysteine, the pH was adjusted to 4 with HCl (1 M) and the reaction was stirred at room temperature for 2 h. The pH was then raised to 6 with NaOH (1 M), and the solution was stirred for an additional hour. The solution was then filtered in sterile conditions and dialyzed with an Amicon Ultra-15 centrifugal filter unit with Ultracell-30 membrane (MWCO 3500) in 4 L containing 1 mM HCl on the first day and 1 mM HCl and 40 g of NaCl on the second and third day. The dialysis was then continued with decreasing salt concentrations in 4 L of double distilled water (30 g – 25 g – 20 g – 15 g – 10 g – 5 g – 0 g – 0 g – 0 g – 0 g). This was then filtered in sterile conditions and lyophilized until it became completely dry.

Coupling Cysteine-Functionalized Polymers to GNPs. To couple GNPs with the cysteine-functionalized alginate-derived polymers (either G-block or medium viscosity high guluronic acid MVG containing polymer), the cysteine-functionalized polymer was reconstituted in double distilled (dd) water (0.5% w/v) and stirred overnight. Gold nanoparticles in solution were then added drop by drop to the stirred polymer solution. The weight ratio of polymer/GNPs was 25:1. GNPs were then centrifuged at 10 000 rpm, washed with dd H_2O, and finally resuspended in dd H_2O.

GNP–Protein Interaction Study. To determine if G-block-coated GNPs adsorb to proteins, quartz crystal microbalance-dissipation (QCM-D) measurements were taken with QSense E4 instrument with a gold crystal sensor, which had a resonance frequency at 4.95 MHz. Bovine serum albumin (BSA) dissolved in PBS (1 mg/mL) was first passed through the sensor module such that BSA forms a well-adsorbed monolayer on the sensor. This was then followed by a wash with PBS and a wash with dd H_2O to remove unbound BSA. A solution of gold nanoparticles was then passed through the sensor module, followed by a water wash to remove unbound GNPs.

Coupling Hylite 750 Hydrazide to G-Block-SH. One hundred milligrams of cysteine-functionalized G-block polymer obtained in the previous step was dissolved in 20 mL of salt buffer (0.1 M MES, 0.3 M NaCl buffer, pH = 6.5) by stirring it overnight at room temperature. Then, 2.081 mg of EDC dissolved in 10 mL of MES-NaCl buffer was added to the aqueous G-block under rapid stirring. This was immediately followed by the addition of 3.675 mg of hydroxy-2,5-dioxopyrrolidine-3-sulfonic acid sodium salt (Sulfo-NHS, Sigma Aldrich 56485) which was dissolved in 10 mL of MES-NaCl buffer. Finally, 2 mg of Hylite 750 hydrazide which had been dissolved in 10 mL of dd H_2O was added to the reaction mixture. This was stirred at room temperature for 20 h. The reaction was then quenched with 1.8 mg of hydroxylamine hydrochloride (Sigma 159417). The solution was then filtered through a 0.22 μm filter under sterile conditions and dialyzed with Amicon Ultra-15 centrifugal filter unit with Ultracell-30 membrane (MWCO 3500) in 4 L with decreasing salt amounts (30 g – 25 g – 20 g- 15 g – 10 g – 5 g – 0 g – 0 g – 0 g – 0 g). The solution was then filtered through a 0.22 μm filter under sterile conditions. This was then freeze-dried until completely dry.

Thermogravimetric Analysis. TGA was performed with a TGA Q5000 V3.10 Build 258 instrument. GNPs were centrifuged and washed twice to remove any excess polymer; the remaining pellet of GNPs was then kept in an oven at 60 °C for 2 h to evaporate water as much as possible. Samples of approximately 0.6 mg were placed in platinum (100 μL) pans, and the temperature was ramped up by 10 °C per minute. For analyzing the polymers alone, they were enclosed with a *TZero* pan and *TZero* lid purchased from TA Instruments, to ensure they do not become volatile with increasing temperatures.

***In Vivo* Study.** To verify the biodistribution and blood pharmacokinetics profile of G-block GNPs, an *in vivo* study was performed. All animal work was performed in compliance with NIH and institutional guidelines. Female C57BL/6J mice aged 10 weeks were used for these studies. The cysteine-functionalized G-block polymers were labeled with Hylite 750 fluorescent dye and coupled to the GNPs. A volume of 0.2 mL of sterile dd H_2O containing 1 mg of G-block-coated GNPs was retro-orbitally injected in mice (n = 8 for each group). All of the injected solutions were sterile filtered prior to injection. Mice were imaged with a Xenogen IVIS using a 720 nm excitation and 820 nm emission. Images of the ventral side of the mice bodies were taken, and mice were shaved on the ventral and dorsal parts of their bodies to minimize attenuation of the fluorescent signal by hair. Blood (60 μL) was also collected from the mice at different time points, and the fluorescence radiant efficiency was measured with the Xenogen IVIS to establish the pharmacokinetics of the G-block GNPs. The blood half-life of the G-block GNPs was estimated by plotting the normalized fluorescence radiant efficiency of the blood (normalized to fluorescence radiant efficiency of the blood of control mice which were injected with 0.2 mL of dd H_2O) *versus* time.

Conflict of Interest: The authors declare no competing financial interest.

Acknowledgment. The authors thank the Wyss Institute for Biologically Inspired Engineering for financial support of this research. The authors also thank Chris Johnson and Dr. Balint Koroskenyi for their help with the use of the equipment at the Wyss Institute Materials Characterization facility. A.K. was a student of the EPFL, Switzerland, and was supported by a predoctoral fellowship from the EPFL WISH FOUNDATION, Switzerland.

Supporting Information Available: Experimental details of the preparation of PEGylated gold nanoparticles; additional results with PEGylated and MVG-coated GNPs; instrument specifications. This material is available free of charge *via* the Internet at http://pubs.acs.org.

REFERENCES AND NOTES

1. Daniel, M.-C.; Astruc, D. Gold Nanoparticles: Assembly, Supramolecular Chemistry, Quantum-Size-Related Properties, and Applications toward Biology, Catalysis, and Nanotechnology. *Chem. Rev.* **2004**, *104*, 293–346.
2. Connor, E. E.; Mwamuka, J.; Gole, A.; Murphy, C. J.; Wyatt, M. D. Gold Nanoparticles Are Taken up by Human Cells but Do Not Cause Acute Cytotoxicity. *Small* **2005**, *1*, 325–327.
3. Aaseth, J.; Haugen, M.; Forre, O. Rheumatoid Arthritis and Metal Compounds—Perspectives on the Role of Oxygen Radical Detoxification. *Analyst* **1998**, *123*, 3–6.
4. Merchant, B. Gold, the Noble Metal and the Paradoxes of Its Toxicology. *Biologicals* **1998**, *26*, 49–59.
5. Zhang, Q.; Iwakuma, N.; Sharma, P.; Moudgil, B. M.; Wu, C.; McNeill, J.; Jiang, H.; Grobmyer, S. R. Gold Nanoparticles as a Contrast Agent for *In Vivo* Tumor Imaging with Photoacoustic Tomography. *Nanotechnology* **2009**, *20*, 395102–395110.
6. Balasubramaniam, S. K.; Yang, L.; Yung, L. Y.; Ong, C. N.; Ong, W. Y.; Yu, L. E. Characterization, Purification, and Stability of Gold Nanoparticles. *Biomaterials* **2010**, *31*, 9023–9030.

7. Eck, W.; Nicholson, A. I.; Zentgraf, H.; Semmler, W.; Bartling, S. Anti-CD4-Targeted Gold Nanoparticles Induce Specific Contrast Enhancement of Peripheral Lymph Nodes in X-ray Computed Tomography of Live Mice. *Nano Lett.* **2010**, *10*, 2318–2322.
8. Chanda, N.; Kattumuri, V.; Shukla, R.; Zambre, A.; Katti, K.; Upendran, A.; Kulkarni, R. R.; Kan, P.; Fent, G. M.; Casteel, S. W.; *et al.* Bombesin Functionalized Gold Nanoparticles Show *In Vitro* and *In Vivo* Cancer Receptor Specificity. *Proc. Natl. Acad. Sci. U.S.A.* **2010**, *107*, 8760–8765.
9. Frens, G. Controlled Nucleation for Regulation of Particle-Size in Monodisperse Gold Suspensions. *Nat. Phys. Sci.* **1973**, *241*, 20–22.
10. Dreaden, E. C.; Mackey, M. A.; Huang, X.; Kang, B.; El-Sayed, M. A. Beating Cancer in Multiple Ways Using Nanogold. *Chem. Soc. Rev.* **2011**, *40*, 3391–3404.
11. Lipka, J.; Semmler-Behnke, M.; Sperling, R. A.; Wenk, A.; Takenaka, S.; Schleh, C.; Kissel, T.; Parak, W. J.; Kreyling, W. G. Biodistribution of PEG-Modified Gold Nanoparticles Following Intratracheal Instillation and Intravenous Injection. *Biomaterials* **2010**, *31*, 6574–6581.
12. Karakoti, A.; Das, S.; Thevuthasan, S.; Seal, S. PEGylated Inorganic Nanoparticles. *Angew. Chem., Int. Ed.* **2011**, *50*, 1980–1994.
13. Anderson, J. M.; Rodriguez, A.; Chang, D. T. Foreign Body Reaction to Biomaterials. *Semin. Immunol.* **2008**, *20*, 86–100.
14. Dami, I.; Hughes, H. G. Effect of PEG Induced Water Stress on *In Vitro* Hardening of Valiant Grape. *Plant Cell, Tissue Organ Cult* **1997**, *47*, 97–101.
15. Roberts, M. J.; Bentley, M. D.; Harris, J. M. Chemistry for Peptide and Protein PEGylation. *Adv. Drug Delivery Rev.* **2002**, *54*, 459–476.
16. Morgan, S. M.; Al-Shamkhani, A.; Callant, D.; Schacht, E.; Woodley, J. F.; Duncan, R. *Int. J. Pharm.* **1995**, *122*, 121–128.
17. Eiselt, P.; Lee, K. Y.; Mooney, D. J. Rigidity of Two-Component Hydrogels Prepared from Alginate and Polyethylene Glycol Diamines. *Macromolecules* **1999**, *32*, 5561–5566.
18. Stockwell, A. F.; Davis, S. S.; Walker, S. E. *In-Vitro* Evaluation of Alginate Gel Systems. *J. Controlled Release* **1986**, *3*, 167–175.
19. Yang, J.; Chen, S.; Fang, Y. Viscosity Study of Interactions between Sodium Alginate and CTAB in Dilute Solutions at Different pH Values. *Carbohydr. Polym.* **2009**, *75*, 333–337.
20. Gu, F.; Amsden, B.; Neufeld, R. J. Sustained Delivery of Vascular Endothelial Growth Factor Using Alginate Beads. *J. Controlled Release* **2004**, *96*, 463–472.
21. Rowley, J. A.; Madlambayan, G.; Mooney, D. J. Alginate Hydrogels as Synthetic Extracellular Matrix Materials. *Biomaterials* **1999**, *20*, 45–53.
22. Ratner, B. D. The Engineering of Biomaterials Exhibiting Recognition and Specificity. *J. Mol. Recognit.* **1996**, *9*, 617–625.
23. Martinsen, A.; Skjäk-Braek, G.; Smidsrod, O. Alginate as Immobilization Material: I. Correlation between Chemical and Physical Properties of Alginate Gel Beads. *Biotechnol. Bioeng.* **1989**, *33*, 79–89.
24. Seely, G. R.; Hart, R. L. The Binding of Alkaline Earth Metal Ions to Alginate. *Macromolecules* **1974**, *7*, 706–710.
25. Klock, G.; Pfeffermann, A.; Ryser, C.; Grohn, P.; Kuttler, B.; Hahn, H. J.; Zimmermann, U. Biocompatibility of Mannuronic Acid-Rich Alginates. *Biomaterials* **1997**, *18*, 707–713.
26. Zhang, W. J.; Laue, C.; Hyder, A.; Schrezenmeir, J. Purity of Alginate Affects the Viability and Fibrotic Overgrowth of Encapsulated Porcine Islet Xenografts. *Transplant Proc.* **2001**, *33*, 3517–3519.
27. Siebers, U.; Horcher, A.; Bretzel, R. G.; Federlin, K.; Zekorn, T. Alginate-Based Microcapsules for Immunoprotected Islet Transplantation. *Ann. N.Y. Acad. Sci.* **1997**, *831*, 304–312.
28. Bouhadir, K. H.; Hausman, D. S.; Mooney, D. J. Synthesis of Cross-Linked Poly(aldehyde guluronate) Hydrogels. *Polymer* **1999**, *40*, 3575–3584.
29. Kohn, R. Ion Binding on Polyuronates-Alginate and Pectin. *Pure Appl. Chem.* **1975**, *42*, 371–397.
30. Smidsrod, O. Molecular Basis of Some Physical Properties of Alginates in the Gel State. *Faraday Discuss.* **1974**, *57*, 263–274.
31. Grasdalen, H. High Field ^{1}H NMR Spectroscopy of Alginate—Sequential Structure and Linkage Conformations. *Carbohydr. Res.* **1983**, *118*, 233–260.
32. Grasdalen, H.; Larsen, B.; Smidsrod, O. P.M.R. Study of the Composition and Sequence of Urinate Residues in Alginates. *Carbohydr. Res.* **1979**, *118*, 255–260.
33. Aida, T. M.; Yamagata, T.; Watanabe, M.; Smith, R. L., Jr. Depolymerization of Sodium Alginate under Hydrothermal Conditions. *Carbohydr. Polym.* **2010**, *80*, 296–302.
34. Bernkop-Schnurch, A.; Kast, C. E.; Richter, M. F. Improvement in the Mucoadhesive Properties of Alginate by the Covalent Attachment of Cysteine. *J. Controlled Release* **2001**, *71*, 277–285.
35. Biebuyck, H. A.; Bain, C. D.; Whitesides, G. M. Comparison of Organic Monolayers on Polycrystalline Gold Spontaneously Assembled From Solutions Containing Dialkyl Disulfides or Alkanethiols. *Langmuir* **1994**, *10*, 1825–1831.
36. Choi, C. H. J.; Zuckerman, J. E.; Webster, P.; Davis, M. E. Targeting Kidney Mesangium by Nanoparticles of Defined Size. *Proc. Natl. Acad. Sci. U.S.A.* **2011**, *108*, 6656–6661.
37. Melacon, M.; Lu, W.; Li, C. Gold-Based Magneto/Optical Nanostructures: Challenges for *In Vivo* Applications in Cancer Diagnostics and Therapy. *Mater. Res. Bull.* **2009**, *34*, 415–421.
38. Mayer, L. D.; Tai, L. C.; Ko, D. S.; Masin, D.; Ginsberg, R. S.; Cullis, P. R.; Bally, M. B. Influence of Vesicle Size, Lipid Composition, and Drug-to-Lipid Ratio on the Biological Activity of Liposomal Doxorubicin in Mice. *Cancer Res.* **1989**, *49*, 5922–5930.
39. Arnida; Malugin, A.; Ghandehari, H. Cellular Uptake and Toxicity of Gold Nanoparticles in Prostate Cancer Cells: A Comparative Study of Rods and Spheres. *J. Appl. Toxicol.* **2010**, *30*, 212–217.
40. Saravanan, M.; Panduranga Rao, K. Pectin–Gelatin and Alginate–Gelatin Complex Coacervation for Controlled Drug Delivery: Influence of Anionic Polysaccharides and Drugs Being Encapsulated on Physicochemical Properties of Microcapsules. *Carbohydr. Polym.* **2010**, *80*, 808–816.
41. Cho, E. C.; Xie, J. W.; Wurm, P. A.; Xia, Y. N. Understanding the Role of Surface Charges in Cellular Adsorption *versus* Internalization by Selectively Removing Gold Nanoparticles on the Cell Surface with a I2/KI Etchant. *Nano Lett.* **2009**, *9*, 1080–1084.
42. Goodman, C. M.; McCusker, C. D.; Yilmaz, T.; Rotello, V. M. Toxicity of Gold Nanoparticles Functionalized with Cationic and Anionic Side Chains. *Bioconjugate Chem.* **2004**, *15*, 897–900.
43. Albanese, A.; Chan, W. C. W. Effect of Gold Nanoparticle Aggregation on Cell Uptake and Toxicity. *ACS Nano* **2011**, *5*, 5478–5489.
44. Navarro, J. R. G.; Plugge, M.; Loumaigne, M.; Sanchez-Gonzales, A.; Mennucci, B.; Debarre, A.; Brouwer, A. M.; Werts, M. H. V. Probing the Interactions between Disulfide-Based Ligands and Gold Nanoparticles Using a Functionalized Fluorescent Perylene-Monoimide Dye. *Photochem. Photobiol. Sci.* **2010**, *9*, 1042–1054.
45. Badia, A.; Cuccia, L.; Demers, L.; Morin, F.; Lennox, R. B. Structure and Dynamics in Alkanethiolate Monolayers Self-Assembled on Gold Nanoparticles: A DSC, FT-IR, and Deuterium NMR Study. *J. Am. Chem. Soc.* **1997**, *119*, 2682–2692.
46. Brewer, S. H.; Glomm, W. R.; Johnson, M. C.; Knag, M. K.; Franzen, S. Probing BSA Binding to Citrate-Coated Gold Nanoparticles and Surfaces. *Langmuir* **2005**, *21*, 9303–9307.
47. Nakata, S.; Kido, N.; Hayashi, M.; Hara, M.; Sasabe, H.; Sugawara, T.; Matsuda, T. Chemisorption of Proteins and Their Thiol Derivatives onto Gold Surfaces: Characterization Based on Electrochemical Nonlinearity. *Biophys. Chem.* **1996**, *62*, 63–72.
48. Silin, V.; Weetall, H.; Vanderah, D. J. SPR Studies of the Nonspecific Adsorption Kinetics of Human IgG and BSA on Gold Surfaces Modified by Self-Assembled Monolayers (SAMS). *J. Colloid Interface Sci.* **1997**, *185*, 94–103.

49. Moulin, A. M.; O'Shea, S. J.; Badley, R. A.; Doyle, P.; Welland, M. E. Measuring Surface-Induced Conformational Changes in Proteins. *Langmuir* **1999**, *15*, 8776–8779.
50. Verma, A.; Stellacci, F. Effect of Surface Properties on Nanoparticle–Cell Interactions. *Small* **2010**, *6*, 12–12.
51. Ademovic, Z.; Klee, D.; Kingshott, P.; Kauffman, R.; Hocker, H. Minimization of Protein Adsorption on Poly(vinylidene fluoride). *Biomol. Eng.* **2002**, *19*, 177–182.
52. Stolnik, S.; Illum, L.; Davis, S. S. Long Circulating Microparticulate Drug Carriers. *Adv. Drug Delivery Rev.* **1995**, *16*, 195–214.
53. Aderem, A.; Underhill, D. M. Mechanisms of Phagocytosis in Macrophages. *Annu. Rev. Immunol.* **1999**, *17*, 593–623.
54. Cedervall, T. Understanding the Nanoparticle–Protein Corona Using Methods To Quantify Exchange Rates and Affinities of Proteins for Nanoparticles. *Proc. Natl. Acad. Sci. U.S.A.* **2007**, *104*, 8691–8696.
55. Nel, A. E.; Madler, L.; Velegol, D.; Xia, T.; Hoek, E. M. V.; Somasundaran, P.; Klaessig, F.; Castranova, V.; Thompson, M. Understanding Biophysicochemical Interactions at the Nano–Bio Interface. *Nat. Mater.* **2009**, *8*, 543–557.
56. Kaufman, E. D.; Belyea, J.; Johnson, M. C.; Nicholson, Z. M.; Ricks, J. L.; Shah, P. K.; Bayless, M.; Pettersson, T.; Feldoto, Z.; Blomberg, E.; *et al.* Probing Protein Adsorption onto Mercaptoundecanoic Acid Stabilized Gold Nanoparticles and Surfaces by Quartz Crystal Microbalance and Zeta-Potential Measurements. *Langmuir* **2007**, *23*, 6053–6062.
57. Park, J.; Park, J. H.; Ock, K. S.; Ganbold, E. O.; Song, N. W.; Cho, K.; Lee, S. Y.; Joo, S. W. Preferential Adsorption of Fetal Bovine Serum on Bare and Aromatic Thiol-Functionalized Gold Surfaces in Cell Culture Media. *J. Colloid Interface Sci.* **2011**, *363*, 105–113.
58. Liu, F.; Li, Y.; Su, X. L.; Slavik, M. F.; Ying, Y.; Wang, J. QCM Immunosensor with Nanoparticle Amplification for Detection of *Escherichia coli* O157:H7. *Sens. & Instrumen. Food Qual.* **2007**, *1*, 161–168.
59. Sonavane, G.; Tomoda, K.; Makino, K. Biodistribution of Colloidal Gold Nanoparticles after Intravenous Administration: Effect of Particle Size. *Colloids Surf., B* **2008**, *66*, 274–280.